

# PREFLIGHT DIAGNOSIS OF MULTICOPTER ACTUATOR FAULT USING SUPERVISED LEARNING WITH DISTURBANCE OBSERVER OUTPUTS

Taegyun Kim<sup>1</sup>, Yeji Kim<sup>1</sup> & Seungkeun Kim<sup>1</sup>

<sup>1</sup>Department of Aerospace Engineering, Chungnam National University

## Abstract

This study proposes a preflight diagnosis method using disturbance observer outputs for health monitoring of multicopter actuators faults. While operating multicopters, determining whether it can perform the flight mission or not is essential. For this reason, we use the disturbance observer's output as a feature for fault diagnosis using artificial neural network. Disturbance observer outputs are used for feature extraction because angular acceleration changes by the rapid attitude movements from actuators faults have the same effect from disturbances. Disturbance observer outputs are obtained according to the actuator fault rates, and the performance of the proposed fault diagnosis is verified via numerical simulations.

**Keywords:** Actuator Fault, Disturbance Observer, Fault Detection and Diagnosis, Unmanned Aerial Vehicle, Supervised Learning, Regression

## 1. Introduction

A unmanned aerial vehicle (UAV) can perform vertical takeoff and landing (VTOL) and hover flight operations. Multicopter UAVs with more than four actuators have actuator redundancy and fault tolerance advantages [1]. However, multicopter UAVs have the disadvantage of having difficulty performing stable flight missions if a problem occurs with the actuator during flight. Multicopter UAVs attain flight using the thrust of actuators only; therefore, thrust faults are directly linked to the total system safety. For this reason, researchers have studied about fault detection and diagnosis (FDD). In addition, since the performance of fault tolerance control is determined according to the FDD model result [2][3], study on a high-accuracy FDD model is being actively conducted. This study uses a disturbance observer in the feature extraction for detecting fault actuator and diagnosing multicopter actuator health.

Generally, the disturbance observer observes uncertainty or disturbances that occur in the system to compensate the baseline controller [4]. Disturbance observers have been used for robust control; however, this paper uses disturbance observer outputs for feature extraction because rapid angular acceleration changes by actuator faults are similar to disturbances. Yujiang Zhong et al. [5] validated the actuator fault detection and diagnosis using estimated disturbance by adaptive augmented state Kalman filter. It is possible to detect and diagnose a single actuator and simultaneous fault, but it is difficult to require an accurate model for the corresponding aircraft. Junghoon Kim et al. [6] developed an actuator fault diagnosis model using the output value of the disturbance observer. The configuration is simple by adding only a disturbance observer, but there is a limitation in that only one actuator is diagnosed. A proposed method in this study is easy to configure as only a disturbance observer needs to be added, and fault detection and diagnosis of all actuators are possible.

This paper is organized as follows: Section 2 introduces the thrust model of a multicopter UAV and shows the feature extraction process using the disturbance observer. Section 3 proposes actuator fault diagnosis model and analyzes its performance based on the performance index. Section 4 offers conclusions of the paper with future work.

## 2. Feature Extraction

This section explains acquiring training data and extracting the features needed to develop the fault diagnostic model.

### 2.1 Actuator Fault Injection

In order to develop an actuator fault diagnosis model using supervised learning, data from various fault situations are needed. In this study, the data is acquired through numerical simulations where the actuator faults occur during flight. Here, training data were acquired while the multicopter hovers with injecting actuator faults. In addition, the command values sent to the actuators were modified to simulate faults wherein normal thrust could not be provided due to propeller damage or faults in the motor [7]. The thrust generated by a single actuator  $T_i$  is as follows [8].

$$T_i = C_T h_i \Omega_i^2 \quad (1)$$

where  $C_T$  is the actuator thrust coefficient, and  $\Omega_i$  is actuator's rotation speed.  $h_i (i = 1 \sim 6)$  is a variable that satisfies  $0 \leq h_i \leq 1$  representing the each actuator efficiency.  $h_i = 1$  means a normal condition, and  $h_i = 0$  means a complete fault. The actuator torque  $Q_i$  due to rotation generated by a single actuator is as follows.

$$Q_i = C_Q h_i \Omega_i^2 \quad (2)$$

where  $C_Q$  is the actuator torque coefficient.

### 2.2 Multicopter Dynamic Model

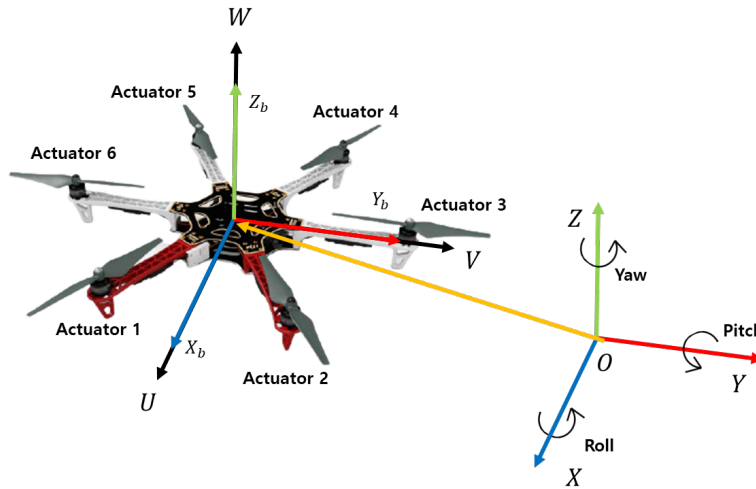


Figure 1 – A multicopter system coordination

A configuration of the multicopter is shown in Figure 1, which is considered as a six degrees-of-freedom.  $X_b, Y_b, Z_b$  axes are originated at the mass center of the multicopter. The  $X$  axis is the forward direction of the multicopter. The multicopter model applied in this study is a hexacopter type and uses six actuators. Therefore, the total thrust can be expressed as follows:

$$\Sigma T_i = C_T \sum_{i=1}^6 h_i \Omega_i^2 \quad (3)$$

When the rotation speed of each actuator is changed, torque is generated for each axis, and roll, pitch, and yaw rotations occur. Figure 2 illustrates the actuator rotation direction and position of the actuators.

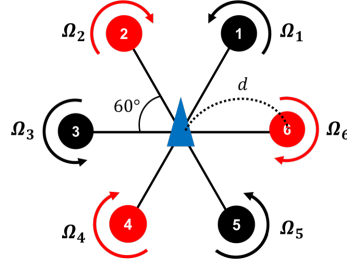


Figure 2 – Multicopter actuator rotation direction

The roll, pitch, and yaw moments are calculated as follows.

$$\begin{cases} \tau_\phi = d_1 C_T (-h_1 \Omega_1^2 + h_2 \Omega_2^2 + h_4 \Omega_4^2 - h_5 \Omega_5^2) + d C_T (h_3 \Omega_3^2 - h_6 \Omega_6^2) \\ \tau_\theta = d_2 C_T (-h_1 \Omega_1^2 - h_2 \Omega_2^2 + h_4 \Omega_4^2 + h_5 \Omega_5^2) \\ \tau_\psi = C_Q (-h_1 \Omega_1^2 + h_2 \Omega_2^2 - h_3 \Omega_3^2 + h_4 \Omega_4^2 - h_5 \Omega_5^2 + h_6 \Omega_6^2) \end{cases} \quad (4)$$

where  $\tau_\phi$ ,  $\tau_\theta$ , and  $\tau_\psi$  are torque output of the roll, pitch, and yaw, respectively.  $d$  is the arm length from the center of the multicopter to the actuator,  $d_1 = d \cos(60)$ , and  $d_2 = d \sin(60)$ .

### 2.3 Disturbance Observer output as a feature

If some of the actuators are faulty, the balance of force is lost instantly, and the multicopter's angular acceleration changes. This phenomenon has a similar effect as changes caused by disturbances. This motivates us to use a disturbance observer as the feature extractor. Figure 3 illustrates a block diagram of the disturbance observer [9].

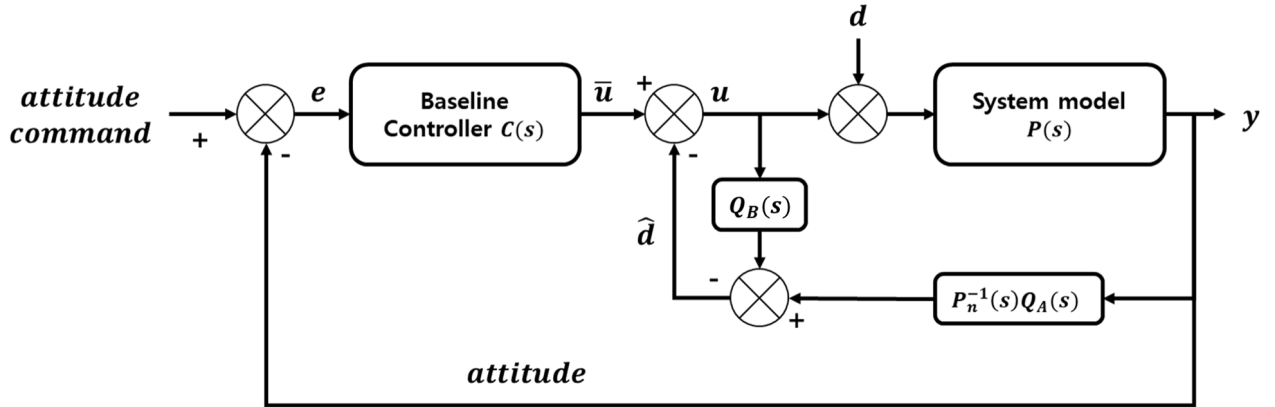


Figure 3 – A diagram of the disturbance observer

In Figure 3,  $C(s)$  is a baseline attitude controller of the multicopter which is configured with the PID controller in this study. The internal structure of the disturbance observer is composed of the multicopter's nominal model,  $P_n(s)$ , and the Q-filters  $Q_A(s)$  and  $Q_B(s)$ . To design the disturbance observer, the nominal model is needed. The nominal model is represented as a simple double integrator from the linearized single-axis moment dynamics,  $J_x \ddot{\phi} = \tau_x$ ,  $J_y \ddot{\theta} = \tau_y$ , and  $J_z \ddot{\psi} = \tau_z$  as follows.

$$P_n(s) = \frac{1}{J s^2} \quad (5)$$

where  $J$  is the moment of inertia in each axis. Suppose that the Q-filter has the same relative degree as  $P_n(s)$  as

$$Q_A(s) = Q_B(s) = \frac{a_0/\tau^2}{s^2 + (a_1/\tau)s + (a_0/\tau^2)}. \quad (6)$$

In Equation 6,  $\tau$  is a positive constant which determines the bandwidth of the Q-filter. As  $\tau$  gets larger, the bandwidth becomes smaller [10]. The disturbance observer receives the control command  $u$  and the multicopter's attitude  $y$ . After that, it estimates the disturbance  $\hat{d}$  by using the inverse dynamics of the nominal model  $P_n(s)$ . The system model  $P(s)$  can be calculated from the multicopter's attitude dynamics in each axis. Figure 4 shows the outputs of the disturbance observer in all actuator fault cases according to the roll and pitch axis.

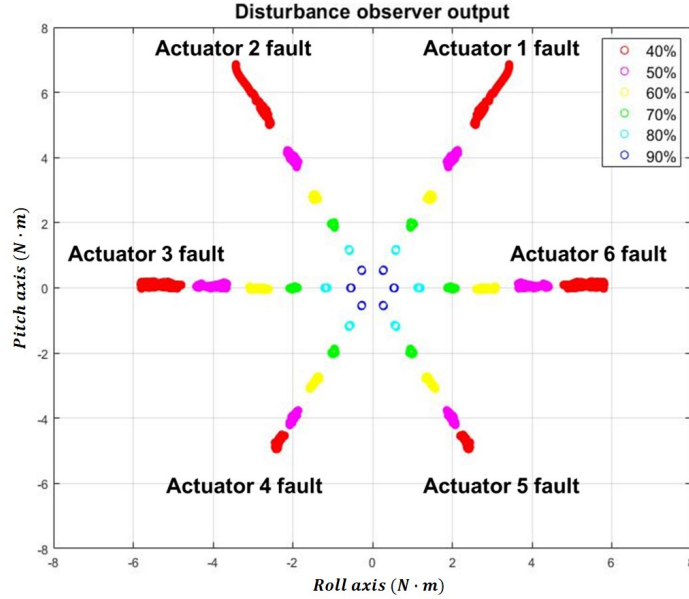


Figure 4 – The disturbance observer outputs in the case of all actuator faults

The disturbance observer outputs are separated according to the degree of fault, and data from the same degree of fault are grouped. In addition, it is confirmed that they are classified according to the fault actuator. This clear distinction means that the disturbance observer outputs indicate the actuator fault rates and are useful for training the actuator fault diagnostic model.

### 3. Fault Detection and Diagnosis Model

For the FDD model, detailed knowledge of the system's internal dynamics is not required. Instead, training data is a source of information about the system. The FDD model learning requires labeling previously occurring fault cases in the training data. This study learns a fault diagnosis model using artificial neural networks (ANN).

#### 3.1 Artificial Neural Network (ANN)

The ANN, known as a multilayer perceptron, consists of a feed-forward architecture of the input, hidden, and the output layer[11]. The output layer nodes corresponds to the classes identified. Figure 5 shows the structure of the ANN with a single hidden layer.

where  $N_i$ ,  $N_H$ , and  $N_O$  are the number of neurons in the input, hidden, and output layer, respectively. In the each node provides a summation of input values  $x_i$ , multiplied by the corresponding weight  $w_{ij}^{(1)}$  between input and hidden layers. The  $j$ -th neuron output of the hidden layer is as follows:

$$s_j^{(1)} = \sum_{i=1}^{N_i} w_{ij}^{(1)} x_i + b_j^{(1)} \quad (7)$$

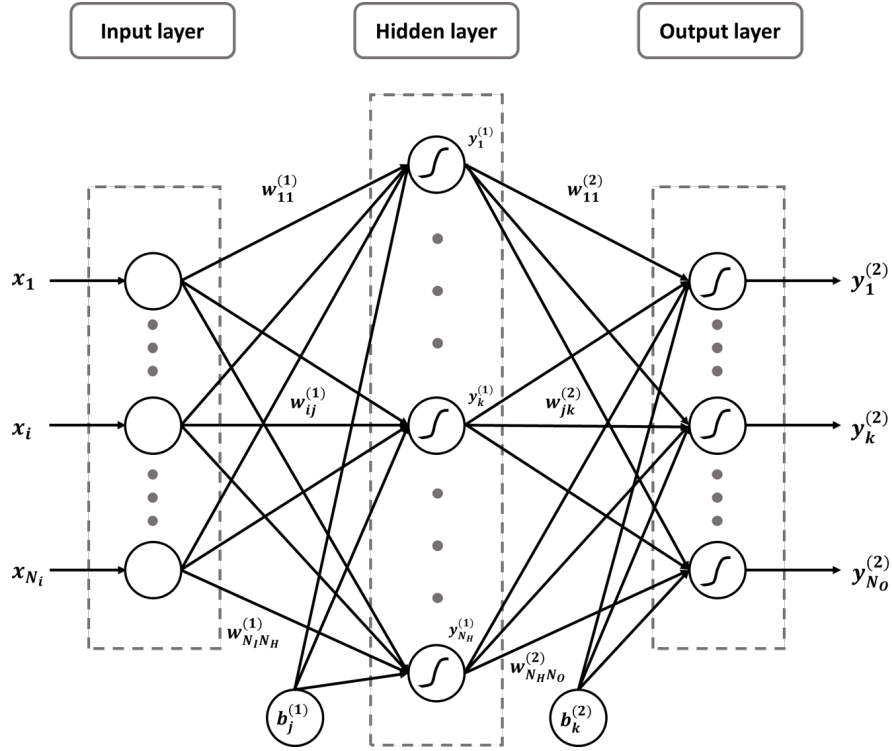


Figure 5 – Typical structure of artificial neural network

The output is obtained by adding the bias term  $b_j^{(1)}$ . The function outputs the sum of the weighted inputs. A sigmoid function is used in this study.  $y_j^{(1)}$  is the output of the hidden layer that  $s_j$  has passed through the sigmoid function; therefore, it can be written as:

$$y_j^{(1)} = f(s_j^{(1)}) = \frac{1}{1 + e^{-s_j^{(1)}}}. \quad (8)$$

The output layer receives  $y_j^{(1)}$  as the input value. The sum of the outputs of the  $k$ -th node neuron of the hidden layer is defined as follows:

$$s_k^{(2)} = \sum_{j=1}^{N_H} w_{jk}^{(2)} y_j^{(1)} + b_k^{(2)} \quad (9)$$

where  $w_{jk}^{(2)}$  is the weight constant between the hidden and output layer, and  $b_k^{(2)}$  is the bias term of the output layer. The results of the output layer passing through the sigmoid function are expressed as follows:

$$y_k^{(2)} = f(s_k^{(2)}) = \frac{1}{1 + e^{-s_k^{(2)}}} \quad (10)$$

Equations (7) – (10) can be expressed by:

$$y_k^{(2)} = f\left(\sum_{j=1}^{N_H} w_{jk}^{(2)} f\left(\sum_{i=1}^{N_I} w_{ij}^{(1)} x_i + b_j^{(1)}\right) + b_k^{(2)}\right) \quad (11)$$

### 3.2 The Structure of the Actuator FDD Model

Fault detection learns which actuator is faulty by receiving the  $\hat{d}_{roll}$  and  $\hat{d}_{pitch}$  values. In the medical examination, the failure actuator number and  $\hat{d}_{roll}$  and  $\hat{d}_{pitch}$  data are received from the failure actuator

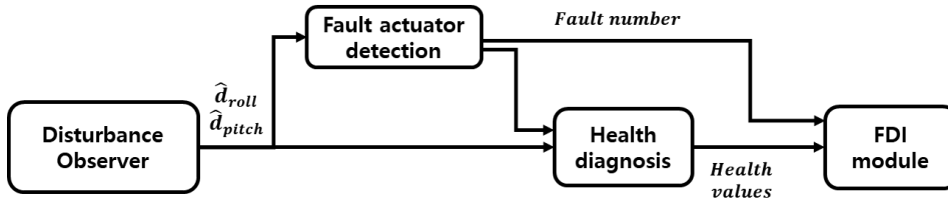


Figure 6 – A block diagram of the actuator FDD model

detection output, and regression learning is performed to output the health value of the actuator. The proposed diagnosis model was learned using 7,200 data which is a summation of 200 data in each section of 40%, 50%, 60%, 70%, 80%, and 90% for each actuator.

### 3.2.1 Fault Actuator Classification Result

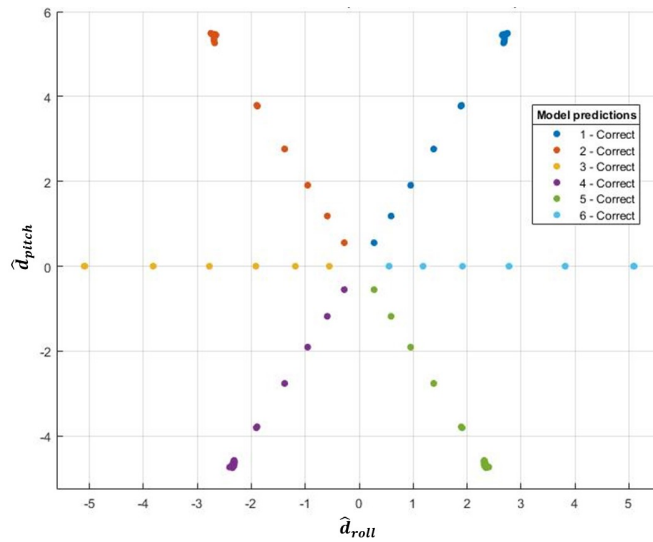


Figure 7 – The results of the classification learning

This section analyzes the results of the proposed fault detection. Figure 7 exhibits a graph of the disturbance observer outputs of roll/pitch during hovering when a each single actuator of the hex-copter has faulted. Actuator faults were injected by reducing the thrstut efficiency by 40% to 90% according to Equation 1. The number in the legend means the number of the actuator that has faulted. In Figure 7, it can be seen that learning has been performed for each actuator fault. Table 1 provides a detailed discussion on the performance evaluation metrics.

Table 1 – Confusion Matrix

		True condition	
		Positive Condition	Negative Condition
Predicted Condition	Total population		
	Positive prediction	True Positive (TP)	False Positive (FP)
	Negative prediction	False Negative (FN)	True Negative (TN)

where "True Positive (TP)" means that the system predicts a faulty actuator as faulty. "True Negative (TN)" represents that a non-faulty actuator is declared as non-faulty. "False Positive (FP)" means that non-faulty actuator is regarded as faulty. Lastly, "False Negative (FN)" implies that a faulty actuator is declared as non-faulty.

Accuracy is calculated as the ratio of predicted observations to the total population by :

$$Accuracy(\%) = \frac{TP + TN}{TP + TN + FP + FN} \times 100 \quad (12)$$

The performance of the fault detection is measured based on True Positive Rate (TPR), False Negative Rate (FNR), Positive Predictive Value (PPV), and False Discovery Rate (FDR). These parameters have been generally used to judge the performance of the Fault detection [12]. These parameters can be defined as follows:

**True Positive Rate (TPR)**

TPR is used to measure the percentage of actual positive candidates :

$$TPR(\%) = \frac{TP}{TP + FN} \times 100 \quad (13)$$

**False Negative Rate (FNR)**

When performing comparisons, FNR represents the probability of incorrectly rejecting the null hypothesis :

$$FNR(\%) = \frac{FN}{TP + FN} \times 100 \quad (14)$$

The system with a higher TPR and lower FNR claims higher efficacy.

**Positive Predictive Value (PPV)**

PPV measures the probability of a false region being predicted as a false :

$$PPV(\%) = \frac{TP}{TP + FP} \times 100 \quad (15)$$

The PPV with a perfect test is 100 %.

**False Discovery Rate (FDR)**

The FDR provides vaule about how many trues have been detected as falses among the overall detected cases :

$$FDR(\%) = \frac{FP}{TP + FP} \times 100 \quad (16)$$

Figure 8a shows the results of TPR and FNR, and Figure 8b shows the PPV and FDR. Table 2 summarizes the TPR, FNR, PPV, and FDR. The 100 % of TPR was accomplished for all actuator fault cases. Also, the proposed method obtained 100% of the PPV. It is confirmed that the proposed fault detection accomplished high accuracy.

**3.2.2 Fault Actuator Diagnosis Result**

Figure 9 displays the results of the health-value regression learning. Figure 9a represents a comparison graph between true and regression learning. It shows little error between the true value and the prediction. As the result of regression learning, it was calculated close to linear. It results from the absence of disturbance other than the actuator fault. Figure 9b means the residuals of the prediction for each actuator fault. In all cases, it is confirmed that the mean residuals of the predicted and true values are 0. The following equations shows index calculation for examining performance by expressing the difference between the true and prediction [13].

**PREFLIGHT DIAGNOSIS OF MULTICOPTER ACTUATOR FAULT USING SUPERVISED LEARNING WITH DISTURBANCE OBSERVER OUTPUTS**

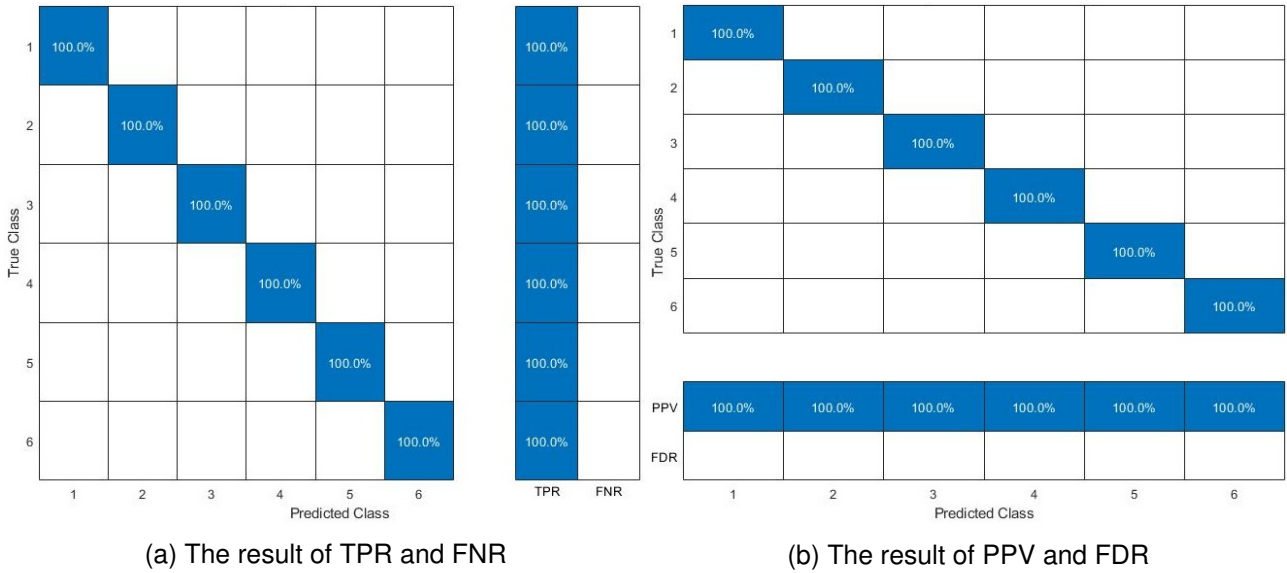


Figure 8 – The fault actuator detection results

Table 2 – The fault detection result by TPR, FNR, PPV, and FDR

Fault actuator number	TPR (%)	FNR (%)	PPV (%)	FDR (%)
Number 1 fault	100 %	0 %	100 %	0 %
Number 2 fault	100 %	0 %	100 %	0 %
Number 3 fault	100 %	0 %	100 %	0 %
Number 4 fault	100 %	0 %	100 %	0 %
Number 5 fault	100 %	0 %	100 %	0 %
Number 6 fault	100 %	0 %	100 %	0 %
Overall performance	100 %	0 %	100 %	0 %

**Mean Absolute of Errors (MAE)**

MAE refers the average values of the absolute difference between true and predicted values in a dataset.

$$MAE = \frac{1}{N} \sum_{i=1}^N |y_i - \hat{y}| \quad (17)$$

where  $y_i$  and  $\hat{y}$  are true and predicted values, respectively, and  $N$  means the total number of data.

**Mean Square of Errors (MSE)**

MSE represents the mean of the squares of the difference between the true and predicted values in a dataset.

$$MSE = \frac{1}{N} \sum_{i=1}^N (y_i - \hat{y})^2 \quad (18)$$

**Root Mean Square of Errors (RMSE)**

RMSE is the square root of MSE. It measures the standard deviation of residuals.

$$RMSE = \sqrt{MSE} = \sqrt{\frac{1}{N} \sum_{i=1}^N (y_i - \hat{y})^2} \quad (19)$$

**R-Squared Score**

## PREFLIGHT DIAGNOSIS OF MULTICOPTER ACTUATOR FAULT USING SUPERVISED LEARNING WITH DISTURBANCE OBSERVER OUTPUTS

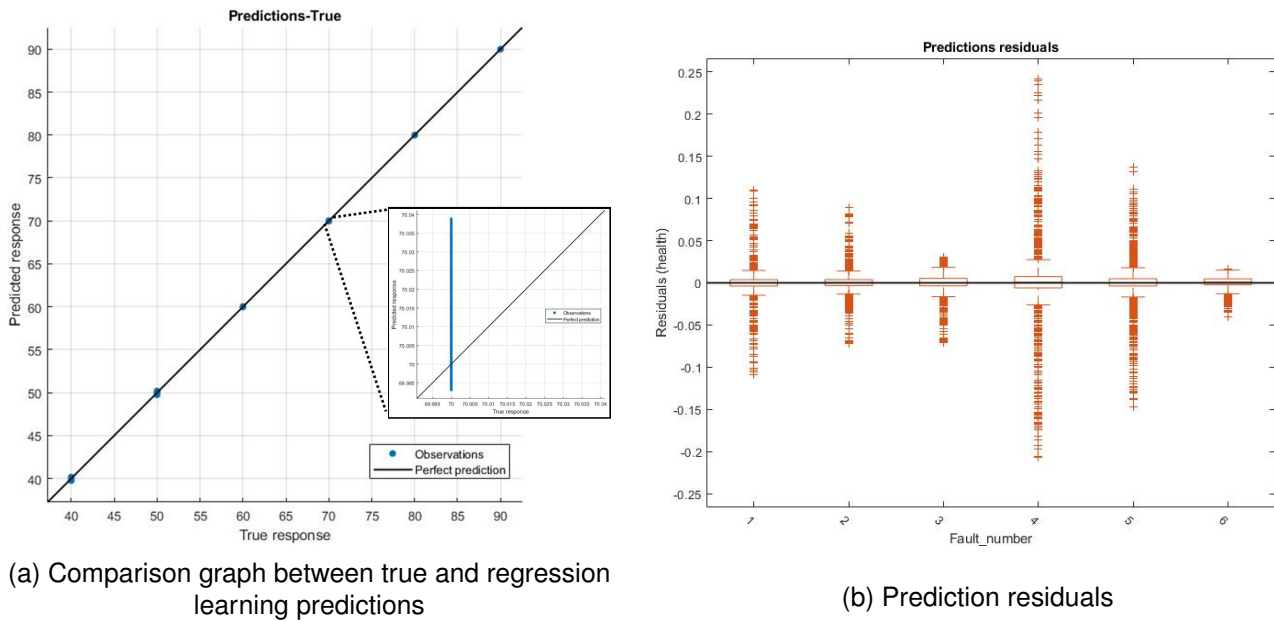


Figure 9 – The result of the health-value regression learning

R-squared represents the ratio of variance of the dependent variable. It is expressed as a number from 0 to 1. if the closer to 1, the better the performance of the regression model.

$$R^2 = 1 - \frac{\sum (y_i - \hat{y})^2}{\sum (y_i - \bar{y})^2} \quad (20)$$

where  $\bar{y}$  means the average vaule of  $y$ . Table 3 shows the performances of regression learning for the health of the actuator.

Table 3 – The regression learning performance values by index

Index	Performance values
MAE	0.030702
MSE	0.003347
RMSE	0.057853
R-Square	1.00

The value of R-square is 1.00, so it can be judged that the regression learning is outstanding. This performance shows that the disturbance observer output can be highly fit for the fault diagnosis of the actuator.

### 4. Conclusions and Future works

The fault diagnostic model of multicopter actuators was developed using artificial neural network. A disturbance observer was used to extract features for utilizing learning model to perform actuator fault detect and diagnosis. The disturbance observer outputs could be used as a reasonable basis for judging the health of actuator fault diagnosis. To verify the performance, a model trained on 7,200 data was tested according to the performance index. As a result, in an ideal environment with no disturbance other than actuator fault, the actuator fault detection and health prediction accomplished high accuracy. In future research, tests will be performed in various environments to verify the performance of the proposed FDD model. Considering disturbances such as wind, we plan to conduct a study to improve diagnosis accuracy even when disturbances other than actuator fault occur.

### 5. Contact Author Email Address

mailto: skim78@cnu.ac.kr (corresponding author)  
 mailto: ktg92@o.cnu.ac.kr

## 6. Acknowledgment

This research was supported by Unmanned Vehicles Core Technology Research and Development Program through the National Research Foundation of Korea(NRF) and Unmanned Vehicle Advanced Research Center(UVARC) funded by the Ministry of Science and ICT, the Republic of Korea(2020M3C1C1A01083162)

## 7. Copyright Statement

The authors confirm that they, and/or their company or organization, hold copyright on all of the original material included in this paper. The authors also confirm that they have obtained permission, from the copyright holder of any third party material included in this paper, to publish it as part of their paper. The authors confirm that they give permission, or have obtained permission from the copyright holder of this paper, for the publication and distribution of this paper as part of the ICAS proceedings or as individual off-prints from the proceedings.

## References

- [1] Kim, T, and Kim. S, "Data-Driven Preflight Diagnosis of Hexacopter Actuator Fault Based on Principal Component Analysis of Accelerometer Signals." *International Conference on Robot Intelligence Technology and Applications. Springer, Cham, 2021.*
- [2] Rudin, Konrad, *et al.*, "Active fault-tolerant control with imperfect fault detection information: Applications to UAVs." *IEEE Transactions on Aerospace and Electronic Systems*, vol. 56, no. 4, pp. 2792–2805, Aug, 2019.
- [3] Li, Bo, *et al.*, "Fault-tolerant attitude stabilization incorporating closed-loop control allocation under actuator failure." *IEEE Transactions on Aerospace and Electronic Systems*, vol. 55, no.4 pp. 1989–2000, Nov, 2018.
- [4] Chen, Wen-Hua, *et al.*, "Disturbance-observer-based control and related methods—An overview." *IEEE Transactions on industrial electronics* vol 63, no.2, pp. 1083-1095, 2015.
- [5] Y. Zhong, Y. Zhang, W. Zhang, J. Zuo and H. Zhan, "Robust Actuator Fault Detection and Diagnosis for a Quadrotor UAV With External Disturbances," in *IEEE Access*, vol. 6, pp. 48169-48180, 2018.
- [6] Kim, J. *et al.*, " Preflight Diagnosis of Multicopter Thrust Abnormalities Using Disturbance Observer and Gaussian Process Regression," *International Journal of Control., Automation and Systems.*, vol. 19, no. 6, pp. 2195–2202, Mar, 2021
- [7] Sadeghzadeh, Iman, *et al.*, " Active fault tolerant control of a quadrotor uav based on gain scheduled pid control." *2012 25th IEEE Canadian conference on electrical and computer engineering (CCECE). IEEE, 2012.*
- [8] T. Kim and S. Kim, "Actuator Fault Diagnosis and Counterplan Using Extended Kalman Filter Considering Symmetry of Hexacopter UAV," *Journal of Institute of Control, Robotics and Systems*, vol. 27, no. 7. *Institute of Control, Robotics and Systems*, pp. 473–481, 31-Jul-2021.
- [9] Li, Shihua, *et al.* Disturbance observer-based control: methods and applications. *CRC press, 2014.*
- [10] Shim, Hyungbo, *et al.*, " Yet another tutorial of disturbance observer: robust stabilization and recovery of nominal performance." *Control Theory and Technology*, vol. 14, no. 3 pp. 237–249, 2016.
- [11] Garcia-Bracamonte, J. E., *et al.*, " An approach on MCSA-based fault detection using independent component analysis and neural networks," *IEEE Transactions on Instrumentation and Measurement*, vol. 68, no. 5, pp. 1353–1361, 2019.
- [12] R. Baly and H. Hajj, "Wafer Classification Using Support Vector Machines," *IEEE Transactions on Semiconductor Manufacturing*, vol. 25, no. 3, pp. 373-383, Aug. 2012.
- [13] Chicco, Davide, *et al.*, "The coefficient of determination R-squared is more informative than SMAPE, MAE, MAPE, MSE and RMSE in regression analysis evaluation." *PeerJ Computer Science* 7, pp.e623, 2021.